Chemical Science

ROYAL SOCIETY OF CHEMISTRY

EDGE ARTICLE

View Article Online
View Journal | View Issue

Cite this: *Chem. Sci.*, 2024, **15**, 18617

All publication charges for this article have been paid for by the Royal Society of Chemistry

Received 24th August 2024
Accepted 6th October 2024

DOI: 10.1039/d4sc05684a

rsc.li/chemical-science

Dynamic organic crystals as exceptionally efficient artificial natural light-harvesting actuators†

Jiaxuan Zhu,‡[a] Wenbo Wu,‡[a] Haoqiang Qi,[a] Yutong Yao,[a] Hui Yu,[a] Xin Huang,[ab] Na Wang,*[ab] Ting Wang*[ab] and Hongxun Hao*[ab]

Dynamic organic crystal materials that can directly convert solar energy into mechanical work hold the potential to be efficient artificial actuators. However, developing dynamic organic crystals that can efficiently transform natural light energy into mechanical energy is still quite challenging. Herein, a novel dynamic organic crystal whose two polymorphs (Form I and Form II) are both capable of effectively converting natural light into work was successfully synthesized. Under the irradiation of ultraviolet (UV), blue and natural light, the on/off toggling of a photosalient effect could be triggered. Specifically, under UV light irradiation, Form I demonstrates output work densities of about 4.2–8.4 × 10^4 J m^{-3} and 1.6–4.9 × 10^2 J m^{-3} before and after disintegration, respectively. Form II exhibits output work densities of about 1.3 × 10^2 to 1.9 × 10^3 J m^{-3} by means of photoinduced bending, suggesting that controllable bending may be more favorable for energy harvesting than the photosalient effect. Utilizing the exceptionally high energy transduction efficiency of Form I, we developed a natural light-driven micro-actuator that can realize output work densities of 2.8–5.0 × 10^4 J m^{-3}. The natural light-harvesting performance of this actuator significantly surpasses those of previously reported photomechanical crystals and could even be comparable to thermal actuators.

1. Introduction

Dynamic organic single crystals are an emerging class of engineering materials with innately valuable properties such as responsiveness, lightweight nature and flexibility.[1–4] In particular, in response to a non-contact stimulus (light),[5–7] some organic single crystals can mimic biological systems in nature to exhibit outstanding dynamic effects such as bending,[8–10] peeling,[11,12] curling,[13] jumping,[14–16] fracturing,[17,18] rolling[19–21] and continuous motion.[19,22,23] Moreover, compared to soft polymer-based materials, organic single crystals have typically shown superior actuator performance (for example, fast response speeds, high energy densities and reasonable photon-to-work conversion efficiencies) due to their abundant intermolecular interactions and ordered structures.[20,24,25] Therefore, organic single crystals with extraordinary actuation properties hold great potential as future energy-harvesting and work-generating materials.[26] Photochromophores that respond to natural light are especially desirable as they avoid the use of harmful ultraviolet (UV) light and can be applicable in devices powered by solar energy,[27–31] which may be an effective way to solve the energy crisis. However, obtaining organic dynamic crystalline materials that can exhibit continuous motion in response to natural light still remains a challenging task. In particular, organic single crystal actuators driven by natural light with high efficiency have rarely been reported.

Based on the time scales of macroscopic motion phenomena, the photoinduced mechanical response can be divided into slow and instantaneous kinematic effects.[32] Photoinduced bending belongs to the slow kinematic effect class, which is realized by applying force to the object through the free end of the crystal, while large stresses will accumulate at the clamped base, which will directly affect the energy transduction and the mechanical work output.[33] Photoinduced (photosalient) jumping is different from photoinduced bending and is a class of instantaneous mechanical effect that is visually more impressive and apparent. As crystals can spontaneously release the accumulated stress and energy in the crystal lattice instantaneously after the induction period, it is generally accepted that photosalient effects are faster than non-salient effects.[14,34,35] However, the power output and energy conversion of organic crystals is influenced by multiple factors, such as the type of phase change or chemical reaction, the source of actuation, reaction groups, chemical family, lattice unit cell

[a]*National Engineering Research Center of Industrial Crystallization Technology, School of Chemical Engineering and Technology, Tianjin University, Tianjin 300072, China*

[b]*China State Key Laboratory of Chemical Engineering, Tianjin University, 300072, China*

† Electronic supplementary information (ESI) available: Experimental section, supplementary figures and movies. CCDC 2376850 and 2376851. For ESI and crystallographic data in CIF or other electronic format see DOI: https://doi.org/10.1039/d4sc05684a

‡ These authors contributed equally.

volume, and static mechanical properties (hardness, Young's modulus).[26] Therefore, a detailed evaluation of the energy conversion efficiency of different mechanical effects would aid the development of crystal actuators.

Dynamic organic single crystals are also promising candidates for the fabrication of soft robots with excellent actuating performance;[36,37] however, the deformation motion of the crystal is severely limited by its brittleness.[38] Although several researchers have made important contributions to the development of flexible crystals and their deformation mechanisms,[39–44] designing and fabricating mechanically flexible organic crystals still remain a challenging task.[45] In addition, the integration of fluorescence properties in dynamic crystal materials is very interesting, allowing intuitive monitoring of changes in the crystal phase.[46] Moreover, dynamic photochromic materials have great potential for applications in intelligent anti-counterfeiting, data recording, information storage and other photonic devices.[47–50] However, dynamic fluorescence switching induced by natural light is still rarely reported.

Herein, we successfully synthesized an acylhydrazone with two polymorphs (Form I and Form II), which could respond to natural light by means of both photosalient and photoinduced bending. The differences in energy conversion efficiency between photosalient and photoinduced bending were revealed and evaluated. Additionally, it is observed that both polymorphs exhibit photochromic and mechanochromic switching luminescence. Ultimately, an application model was proposed to demonstrate that the dynamic crystal could be a promising candidate for high-efficiency microactuators driven by natural light.

2. Results and discussion

(*E*)-4-Chloro-*N*′-(4-(dimethylamino)benzylidene)benzohydrazide (CDBB) (Fig. 1a) was synthesized *via* a straightforward Schiff base reaction; the detailed synthetic procedures are provided in the ESI.† The chemical structures were confirmed using ^{1}H and ^{13}C NMR spectra (Fig. S2 and S3†). Upon *n*-hexane diffusion into a dichloromethane solution, colorless crystals with plate and acicular morphologies were obtained. To determine whether these crystals had different crystal structures, powder X-ray diffraction (PXRD), differential scanning calorimetry (DSC) (Fig. S4†), and single-crystal X-ray diffraction (SCXRD) were conducted, revealing that they are indeed two distinct polymorphs, designated as Form I (plate-like crystals) and Form II (acicular crystals).[51,52] The fluorescence properties of the two polymorphs were also examined, and it was observed that the emission peaks of Form I and Form II appeared at 450 nm and 452 nm with PL lifetimes of 1.18 and 0.61 ns, respectively (Fig. S5a†). Furthermore, the fluorescence quantum yields (PLQYs) of Form I and Form II are 1.0% and 0.9%, respectively. Surprisingly, it was found that both polymorphs exhibited broad UV-vis absorption in the range of 200 nm to 500 nm, suggesting their potential for inducing photomechanical responses under LEDs, such as 365 nm and 425 nm, or even natural light (Fig. S5b†).

Acylhydrazone derivatives are known for their potential to undergo reversible photoisomerization due to the presence of a –C=N– moiety.[53,54] Given that the photomechanical effect can be influenced by intermolecular interactions and packing modes, the photoactuation characteristics of the two polymorphs were investigated. As shown in Movie S1,† it was observed that, when the major facet (001) of Form I (*L*, *W*, *T*: 2400 μm, 80 μm, 35 μm) was exposed to 365 nm (160 mW cm^{-2}) UV light, it exhibited an instantaneous ballistic motion such as popping and jumping (Fig. 1b and d). Recordings of this phenomenon in Form I using a high-speed camera revealed that the photosalient effects occurred within 8.3 ms (Movie S2 and Fig. S6†). Furthermore, an increase in laser intensity (320 mW cm^{-2}) resulted in a significantly reduced response time and increased the macroscopic speed of the jumping. Form I also demonstrated a strong photosalient effect in response to visible light (425 nm, 160 mW cm^{-2}) (Movie S1† and Fig. 1e), with a relatively delayed response time compared to high-energy UV light. It was speculated that this crystal could probably also respond to natural light. To confirm this hypothesis, the behavior of Form I was further investigated under natural light. Notably, Form I also exhibited excellent photoinduced jumping effects under natural light, which is a relatively rare phenomenon (Fig. 1f and Movie S3†). When the major facet (001) was exposed to natural light, Form I bent away from the light (within 30 s) and eventually leapt and split into several pieces (Movie S3 and Fig. S7†). This suggested that CDBB could act as a potential candidate for the conversion of natural light to mechanical energy.

In contrast, the needle-like Form II displayed a gentler photomechanical effect compared to Form I, without obvious fragmentation. We found that all three types of light sources with the same intensity could induce significant backlight bending of Form II (with a curvature of about 40°) (Fig. 1c, g–i and Movie S4†). Practically, it has been reported that the crystal size can affect the photomechanical effects of crystals; thus, the photomechanical effects of the two polymorphs were observed at a larger size.[33] Form I (*L*, *W*, *T*: 3000 μm, 100 μm, 50 μm) exhibited slight bending with subsequent jumping, while Form II (*L*, *W*, *T*: 3000 μm, 55 μm, 50 μm) still bent away from the light, but at a greatly decreased speed (4° s^{-1} under UV light). Thus, Form I was considered to be a typical photosalient crystal. Additionally, the response time of the crystal decreased as the wavelength of the light source shortened, likely because the photochemical reactions were more easily triggered under high-energy irradiation. Moreover, plastically bent Form II could slightly stretch after being heated to 120 °C (Fig. S8†). It was anticipated that the single crystal might undergo motions with different response times under different light sources, providing potential for controlling the mechanical response by modulating the wavelength of the irradiating light.

To further investigate the different behaviors of the two polymorphs, the photoisomerization of the CDBB molecules was examined using UV-vis absorption spectroscopy and Fourier-transform infrared spectroscopy (FTIR) (Fig. 2a, b and S9–S11†). Considering Form I for instance, its maximum absorption band at 380 nm decreased in intensity, while the

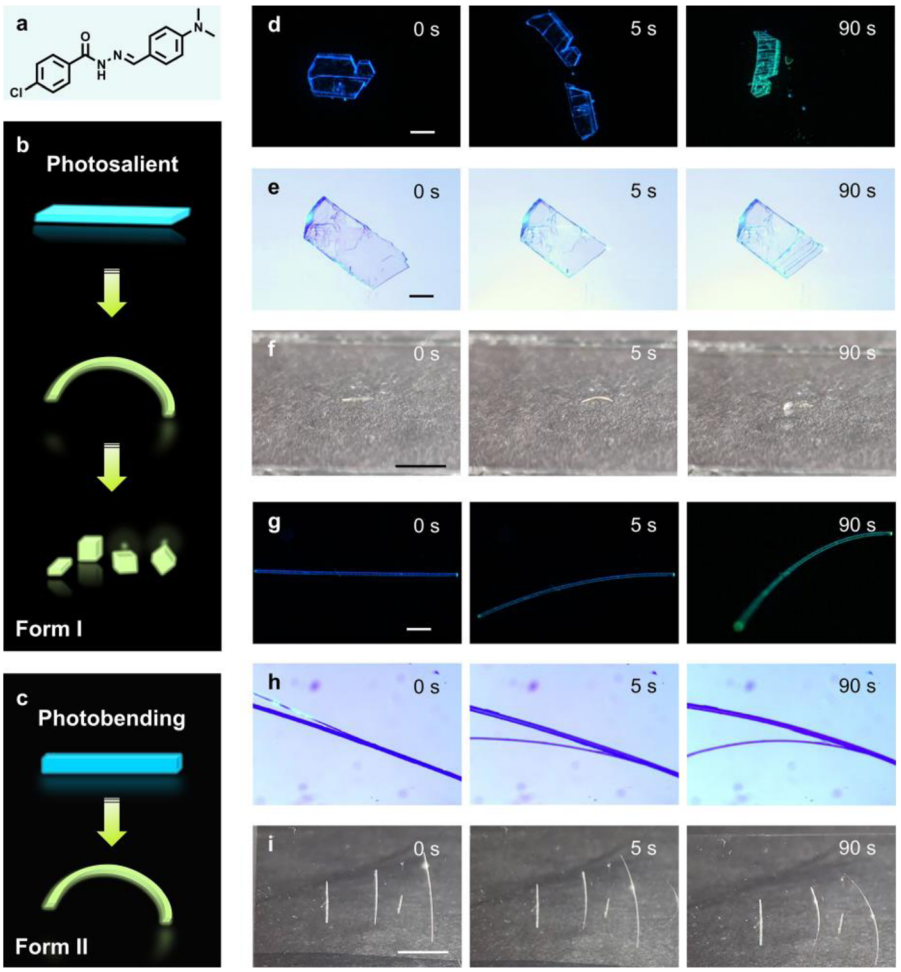

Fig. 1 (a) Chemical formula of CDBB. (b and c) Schematic diagrams of the photosalient and photoinduced bending process. (d–f) Images of the photosalient crystals under visible and UV light: 365 nm (d), 425 nm (e), and natural light (f). (g–i) Images of the photoinduced bending crystals under visible and UV light: 365 nm (g), 425 nm (h), and natural light (i). The scale bar is 200 μm (d, e, g and h) and 1 cm (f and i).

enhancement at around 450 nm was observed (Fig. 2a). These spectral changes were ascribed to (*E*)-to-(*Z*) photoisomerization,[55] and the absorption intensity slightly increased when the irradiation time was prolonged, reaching its maximum after 120 s (Fig. S11†). Furthermore, the FTIR data also implied a change in structure occurred after irradiation. It can be seen that the characteristic peaks at 1650 cm^{-1}, associated with the stretching vibration of ν(C=N), slightly shifted indicating the occurrence of photoinduced *cis–trans* isomerization. In addition, PXRD was also conducted on different samples, and it was found that the peak belonging to the (011) facet disappeared upon irradiation, while a new peak belonging to the (001) facet appeared instead (Fig. S12a†). This suggested that the photoisomerization also caused structural changes.

It is well-known that the bending mechanism is usually simplified as a "bimetallic mechanism" (Fig. 2c and d).[56,57] Based on this theory as well as the above characterization, the mechanism of photoinduced bending of Form I is discussed.[9] Firstly, the molecular volume changes induced by light were calculated based on the Bondi atomic van der Waals radius.[58] It was revealed that an increase in molecular width by 37.99% (+2.762 Å) was found after the $E \rightarrow Z$ isomerization (Fig. S14†). This would further lead to an elongation of the *a*-axis. It was hypothesized that, when the (001) facet is irradiated, the crystal expanded along the *a*-axis, causing the crystal to bend away from the light (Fig. 2d). Additionally, thicker crystals of Form I might directly split or jump due to greater accumulated strain, according to the Euler–Bernoulli equation.[59] However, thick crystals of Form II remained plastically bent, just as thin crystals of Form II did. The difference in the behaviors of the two forms depends on the release mode of the accumulated strain, which can be influenced by intermolecular interactions and the molecular stacking arrangement.[60] Therefore, a more detailed analysis on the crystal structure of the polymorphs was conducted.

Herein, the crystal structures of the two polymorphs were determined to gain insight into the reasons for the differences in the photomechanical responses. Form I crystallizes into a triclinic system (a = 5.2898(2) Å, b = 7.8669(3) Å, c = 17.5590(6) Å, α = 99.161(3)°, β = 96.187(3)°, γ = 90.692(3)°), where the dihedral angle between the two aromatic rings is 117.64°. In contrast to Form I, Form II belongs to the

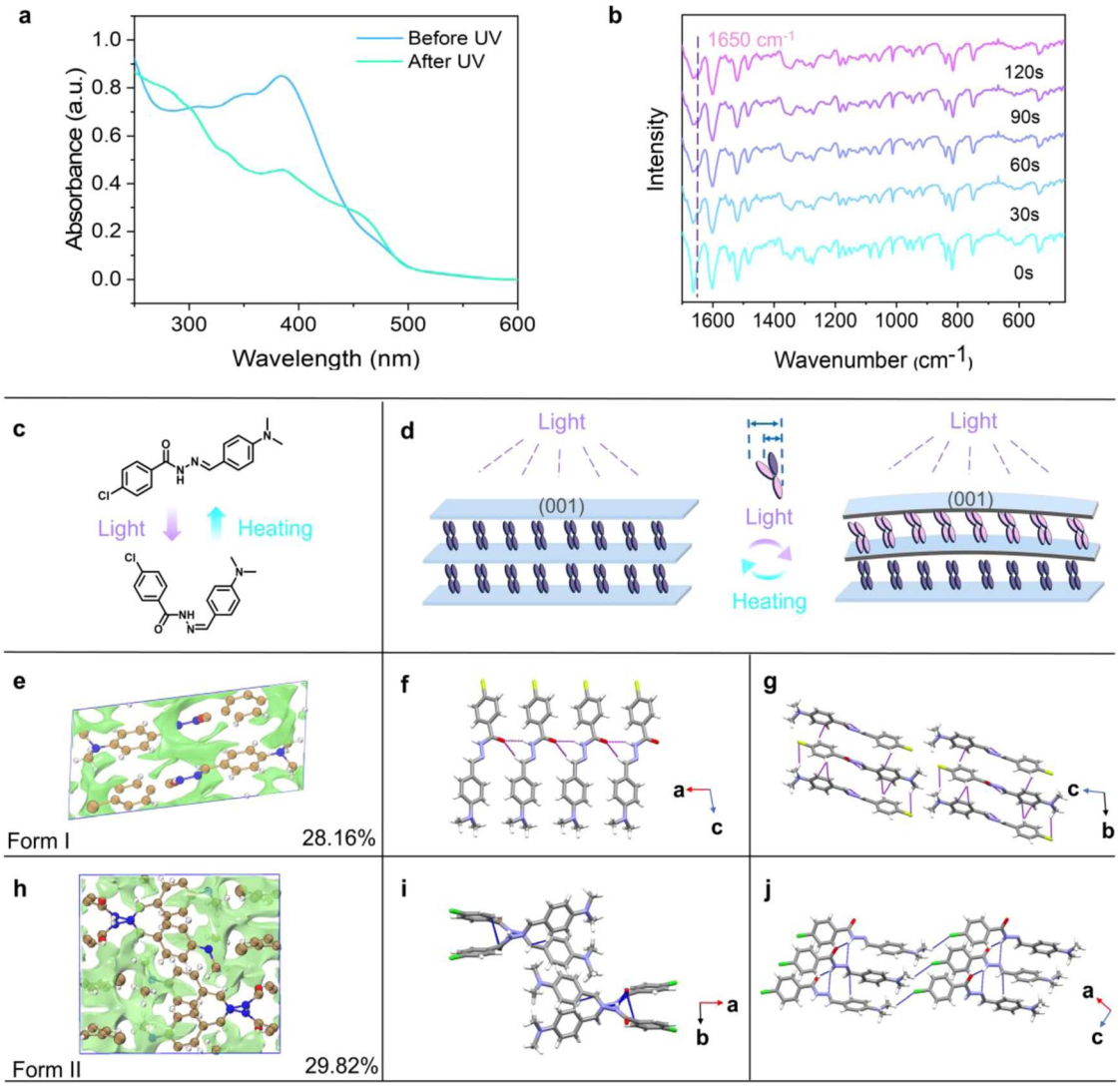

Fig. 2 (a) Absorption spectra of pristine and irradiated samples of Form I. (b) FTIR spectra of irradiated Form I taken at 30 s time intervals. (c) Schematic diagram of CDBB before and after isomerization. (d) Schematic of the mechanism for the photoinduced bending of the Form I and Form II crystals. (e–g) Fractional free volume and intermolecular interactions of Form I. (h–j) Fractional free volume and intermolecular interactions of Form II.

monoclinic system (a = 14.9184(5) Å, b = 12.9302(4) Å, c = 7.6631(3) Å, β = 96.635(3)°), and the dihedral angle between the two aromatic rings is 106.84° (Table S1†). The photoisomerization energy barriers of the CDBB molecules in Form I and Form II were calculated to be 44.82 kJ mol^{-1} and 43.17 kJ mol^{-1}, respectively. Furthermore, the fractional free volume (FFV) is often used to characterize the difficulty of photoisomerization, where a large free space usually suggests that isomerization is more likely to happen. It turned out that the FFV values of Form I and Form II are 28.16% and 29.82%, respectively, according to promolecular density analysis (Fig. 2e, h and Table S2†). The similarities in the isomerization energy barrier and FFV values could not explain the distinct differences observed in the photomechanical effects. Therefore, the intermolecular interactions and molecular packing were further analyzed.

For Form I, the CDBB molecules form stack columns through strong N–H···O (D, d, θ = 3.067 Å, 2.242 Å, 156.02°) and C–H···O (3.242 Å, 2.448 Å, 141.03°) hydrogen bonds along the a-axis (Fig. 2f and g). The adjacent molecular columns are further connected by C–H···π (3.611 Å, 2.770 Å, 148.02°, and 3.583 Å, 2.770 Å, 141.54°) interactions along the b-axis, contributing to the plate-like crystals. For Form II, adjacent CDBB molecules form an aggregation chain structure through N–H···O (2.8998 Å, 2.037 Å, 161.11°), N–H···N (3.318 Å, 2.675 Å, 129.60°) and C–H···π (3.369 Å, 2.759 Å, 122.70°) interactions, and adjacent aggregation chains are further connected by C–H···Cl (3.567 Å, 2.842 Å, 131.47°) interactions along the c-axis, resulting in acicular crystals (Fig. 2i and j). It has been confirmed that the photochemical behaviors originate from the isomerization of the –C=N– moiety. Based on the above crystal structure analysis, it can be found that the *cis–trans* isomerization of Form I is mainly

limited by the C–H···O and N–H···O hydrogen bonds, while the *cis–trans* isomerization of Form II is limited not only by N–H···N and N–H···O hydrogen bonds, but also by C–H···π interactions (Fig. S15†). Therefore, the isomerization rate of Form I with fewer intermolecular interaction restrictions might be faster compared to that of Form II. Consequently, faster energy storage and release might be the main reason for the photo-salient effect of Form I.

Apart from photomechanical properties, both polymorphs of CDBB also demonstrated photochromic fluorescence switching effects in the solid state. The original crystals of both polymorphs emitted bright blue light centered at 452 nm and 454 nm (λ_{ex} = 365 nm) (Fig. 3a), with lifetimes of 1.18 and 0.61 ns, respectively. Under 365 nm light irradiation, the emission peaks gradually shifted towards green emissions at 504 nm and 508 nm (Fig. 3b, c and S16†), with corresponding lifetimes of 1.49 and 2.32 ns (PLQYs = 5.0% and 4.6%, respectively). The crystals also exhibited significant photochromic fluorescence switching even under irradiation of 425 nm or natural light. It has been hypothesized that the photochromic behavior might be attributed to the conformational isomerization of the –C=N– groups.[61,62] To gain further insights into the processes of excitation and emission, the electronic structures of the *trans*- and *cis*-isomers of both polymorphs were simulated using DFT calculations as well as time-dependent density functional theory (TD-DFT) calculations. It was indicated that, compared to the *trans* fragments, the emissions of the *cis* fragments were significantly redshifted (3.61 → 3.70 eV; 3.51 → 3.69 eV), aligning with the experimentally observed phenomena. Additionally, this high-contrast luminescent change is reversible. The irradiated sample was heated at 80 °C for 10 min and then examined using PXRD and UV-vis spectroscopy. As illustrated in Fig. S12 and S17,† the PXRD curves and UV-vis results of the heated samples closely resembled those before irradiation, which proved that the crystal could restore its original state by exposure to short-term heating.

Additionally, both polymorphs also demonstrated remarkable mechanochromic fluorescence switching characteristics with high contrast and instantaneous responses. The fluorescence emissions of ground samples of both polymorphs rapidly changed from blue to cyan (Fig. 3d). As shown in Fig. 3d, the emission peaks of Form I and Form II shifted to 489 nm and 499 nm, with lifetimes of 2.20 and 3.05 ns (PLQYs = 5.7% and 6.0%, respectively). PXRD analysis of the ground samples revealed the disappearance of certain diffraction peaks (2θ = 7.81, 15.00, 15.90) (Fig. 3e and S18b†),[63] suggesting that the crystal structure changed upon grinding. Therefore, it can be inferred that the red shift in emission might result from the partial disruption of the intermolecular hydrogen bonds and packing modes. Analysis of the DSC data indicated that the melting point was not affected upon grinding, while the phase transition temperature shifted from 186.50 °C to 173.60 °C, indicating that Form I transformed to an unknown polymorph upon grinding (Fig. 3f). Form II showed a similar trend to Form I upon grinding, as illustrated in Fig. S18c.†

To our surprise, Form II also exhibited significant elasticity along the major facet (010) upon exposure to mechanical force and could regain its straightness once the external force was

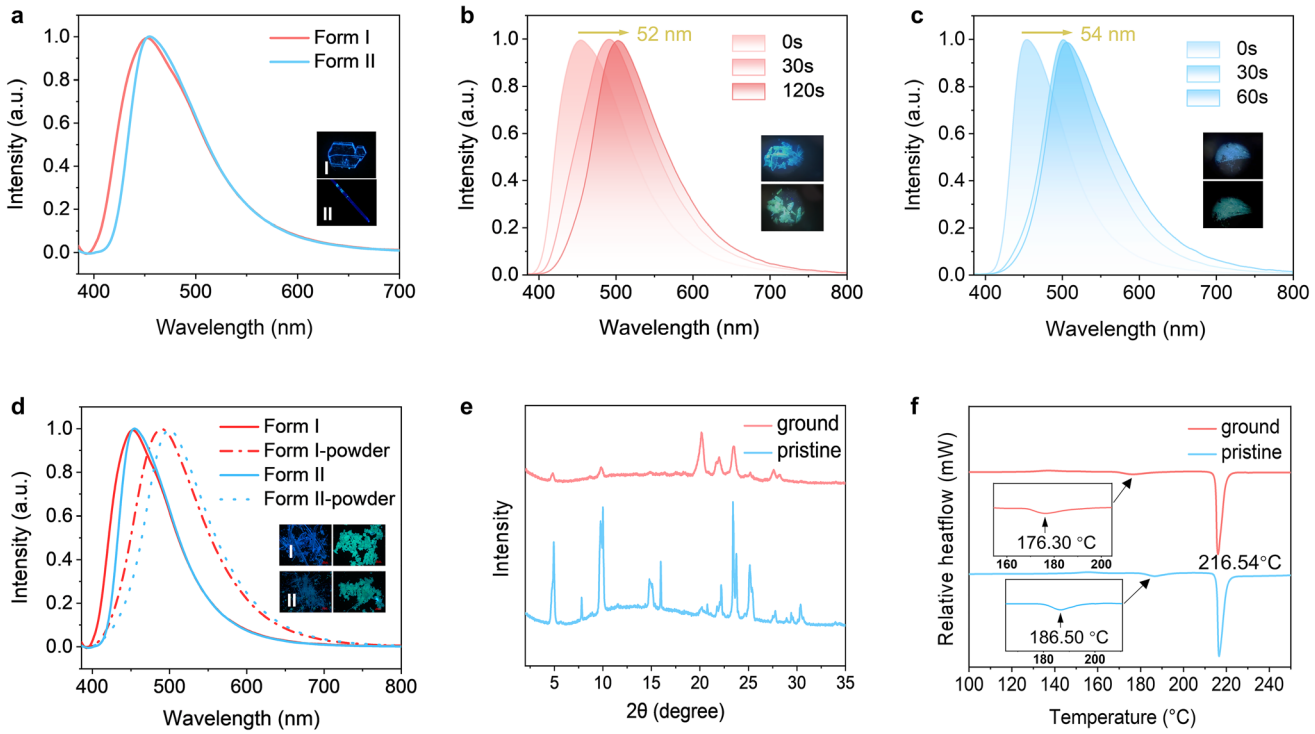

Fig. 3 (a–d) PL spectra and luminescent photographs of: Form I and Form II (a), Form I under 365 nm UV light irradiation (b), Form II under 365 nm UV light irradiation (c), and ground Form I and Form II (d). (e) PXRD patterns of Form I and the ground samples. (f) DSC curves of Form I and the ground samples.

removed (Fig. 4a and Movie S5†). The typical single crystal elastic strain limit of Form II was calculated to be 3.7% (Fig. S20†). Once the strain exceeded the threshold value, the crystal would fracture. The basic mechanical properties of Form II were analyzed using nanoindentation testing, with the elastic modulus and hardness being 12.60 GPa and 0.35 GPa, respectively (Fig. S21†). The high elastic modulus and low hardness indicate its excellent deformation ability and mechanical flexibility.

To clarify the possible mechanism of elastic deformation of Form II, a structure analysis was conducted. Viewed along the *c* axis, the molecules form strong aggregation chain structures *via* hydrogen bonding, and adjacent aggregation chains are further connected by vdW interactions, (E_{total} = −40.2 kJ mol^{-1}, −117.5 kJ mol^{-1} and −178 kJ mol^{-1} along the crystallographic *a*, *b* and *c* axes, respectively) (Fig. 4b, S22 and S24†). Generally, it is acknowledged that elastic deformation allows the reorganization of molecular arrangements during deformation,[2] such as slight rotations and translations to accommodate stress variation. Obviously, unlike previously reported elastic crystals, π–π stacking interactions are absent in Form II. Therefore, it can be speculated that the strong aggregation chains connected by hydrogen bonds can also serve as springs to expand along the exterior arc while contracting along the interior arc, promoting elastic bending of the crystals (Fig. 4c).[64]

Dynamic organic crystals are a class of emerging energy conversion materials and have not yet been developed into practical actuators. It is difficult to fully evaluate the driving efficiency of a crystal, which restricts the development of crystal actuators with high-efficiency actuating performance.[33] In this study, we quantitatively characterized the power output and energy conversion efficiency of the polymorph-dependent on/off photo-salient effect of CDBB, by focusing on the factors affecting energy conversion. To prevent crystal leaping and popping under light irradiation, a glass sheet was placed on each side and above the Form I crystal (*L*, *W*, *T*: 3500 μm, 70 μm, 40 μm) (Fig. 5a and Movie S6†), and the output force and output force density were calculated using eqn (1) and (2):

$$F_{out} = \mu mg \quad (1)$$

$$F^{v}_{out} = \frac{F_{out}}{V}. \quad (2)$$

The coefficient of static friction between the glass sheets was represented by μ, while the mass of the glass plate was denoted as *m*. The output force density was expressed as F^{v}_{out}. As one side

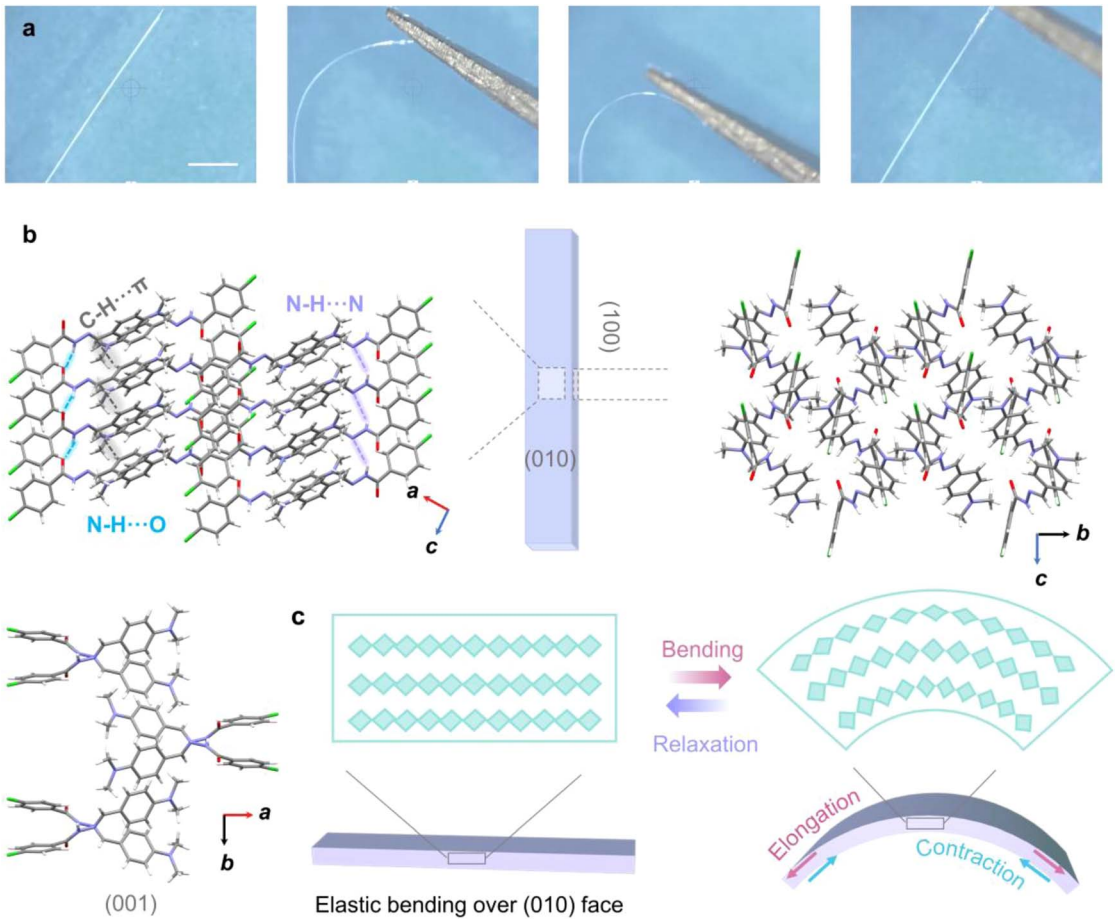

Fig. 4 (a) Elastic bending processes of the Form II crystals along the (010) facet. (b) Molecular packing and intermolecular interactions of Form II. (c) Schematic diagram showing the changes of the molecules inside the crystal during elastic bending. The scale bar is 200 μm.

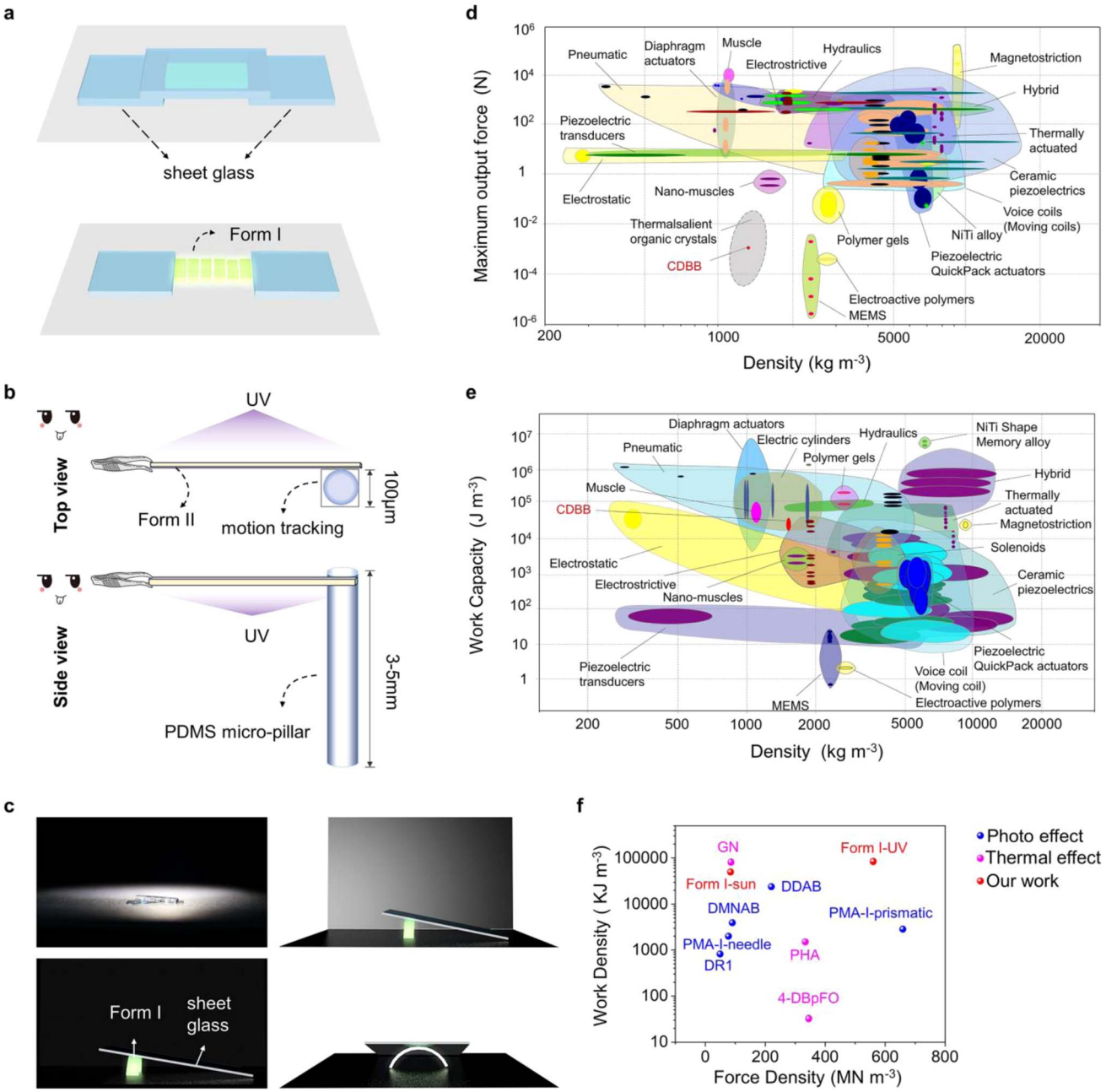

Fig. 5 (a) Schematic illustration of the setup used to assess the actuation performance of disintegrated Form I crystals. (b) Diagram showing the setup used to track the displacement of the PDMS micropillar tips. (c) Schematic illustration of the setup used to assess the actuation performance of Form I crystals before disintegrating. (d and e) The output force and work density *versus* density of Form I under natural light co-plotted with other main actuator classes. (f) Actuation performance compared with other crystals.

of the glass plate was fixed, the output work and work densities were calculated based on the displacement (L) of the other side of the glass plate (3) and (4):

$$W_{out} = F_{out}L \quad (3)$$

$$W_{out}^{v} = \frac{W_{out}}{V}. \quad (4)$$

The needle-like Form II (L, W, T: 4200 μm, 40 μm, 35 μm) generated a bending force during the photoreaction process. To amplify this force, we designed a device with PDMS micro-columns that could be curved (diameter: 100 μm) (Fig. 5b and Movie S7†). Dynamic performance indicators for the bent crystals were established by tracking the displacement of the column tips. This allowed us to determine the force exerted by the crystal on each column as well as the work generated:

$$F_{out} = k\delta \quad (5)$$

$$W_{out} = F_{out}\delta. \quad (6)$$

The stiffness of the microcolumn, denoted as k, was calculated using the Young's modulus of PDMS ($E_{PDMS} = 2.6$ MPa), and the displacement of the column tip was denoted as δ. Furthermore, in order to assess the energy conversion efficiency, the use of output power as a standard measurement was also incorporated, while the input light source was kept consistent.

$$P_{out}^{v} = \frac{W_{out}^{v}}{t} \quad (7)$$

These properties were then normalized by volume to obtain scale-independent properties such as force density, work density, and power density. As shown in Table S5,† it was revealed that the disintegration of Form I had a higher output force density (1.2×10^7 N m^{-3}) compared to the bending of Form II (1.8×10^5 N m^{-3}), while the work density and power density of Form I (3.3×10^2 J m^{-3} and 9.1×10^1 W m^{-3}) were lower than that of Form II (7.3×10^2 J m^{-3} and 1.0×10^2 W m^{-3}, respectively). Given that the disintegration of Form I could hinder the analysis, it is necessary to evaluate the energy conversion efficiency of the crystal before disintegration, and hence a device to do this was designed (Fig. 5c and Movie S8†). The crystal size (L, W, T: 4000–5000 μm, 70–80 μm, 40–50 μm) was controlled in order to induce bending rather than direct disintegration. The force exerted by the crystal on the glass was determined by measuring the increase in height of the glass's center of gravity, which was calculated by measuring the angle θ between the glass sheet and the ground:

$$F_{out}\frac{h}{\tan\theta} = \frac{mgL}{2}\cos\theta \quad (8)$$

$$W_{out} = \frac{mgL}{2}\sin\theta \quad (9)$$

Based on this method, it was calculated that Form I was capable of generating a force density, work density, and power density of 5.0×10^8 N m^{-3}, 6.0×10^4 J m^{-3}, and 1.2×10^4 W m^{-3}, respectively, before disintegration, which are much higher than the disintegration of Form I and the bending of Form II (Table S6†). In fact, we speculate that the crystal might have a higher energy conversion efficiency in the photosalient process, while the force was dissipated by the dispersed individual motion direction, preventing a large amount of kinetic energy from being converted into work. Therefore, the salient effect was inefficient and not conducive to energy collection and utilization. Furthermore, it was found that Form I could be induced to bend rather than shattering by controlling the crystal size. The continuous bending process caused by stable strain accumulation allowed for centralized and controllable force output, making it a potential candidate for light-driven actuators.

Given that the Form I of the CDBB molecule has extremely high efficiency under UV light irradiation, we imagine that it can also be used as an effective device for solar energy utilization and conversion. As shown in the Fig. S26,† we demonstrate that Form I functions as a micro-lifting robot that utilizes natural light to lift heavy objects (Movie S9†). Experiments were carried out under sunlight using the device in Fig. 5c, which allowed the crystals to lift a glass sheet to a certain height. The dynamic performance of Form I under natural light irradiation was also quantified, revealing a force density range of 6.9–8.4 × 10^7 N m^{-3}, which is significantly higher than many actuators and similar to smaller MEMS-based devices, electroactive polymers, and even some thermosalient organic crystals (Fig. 5d and Table S6†).[65] Additionally, the work density range of 2.8–5.0 × 10^4 J m^{-3} significantly surpasses that of previously reported photomechanical crystals and is competitive with thermal and diaphragm actuators, indicating the potential of the polymorphs for high working outputs (Fig. 5e, f and Table S6†).[66] These findings demonstrate the excellent competitiveness of the obtained crystals to be used as solar-driven components.

3. Conclusions

In this study, we successfully synthesized a novel photoresponsive crystal with two polymorphs. The distinct photomechanical motions of the two polymorphs are triggered by the *cis–trans* isomerization of acylhydrazone groups, which could be induced by both UV and natural light. Notably, Form I, which lacks C–H···π interactions, displays intriguing photosalient behavior, while Form II is constrained to bend away from light. Given that both effects involve energy conversion from light to mechanical work, we designed several setups to compare their energy conversion efficiencies. Form I demonstrates a work density of about 4.2–8.4 × 10^4 J m^{-3} and 1.6–4.9 × 10^2 J m^{-3} before and after disintegration, respectively, which is attributed to a rapid energy release process. This excellent efficiency allows Form I to work as a solar-driven microcomponent that can rival some conventional actuators, such as muscle and electric cylinders. This work not only validates the feasibility of converting natural light into work through straightforward photochemical reactions but also offers valuable insights into the relationship between structural properties and photomechanical effects.

Data availability

Crystal data for Form I and Form II are available from the Cambridge Crystallographic Data Centre with reference numbers 2376850 and 2376851. All data are available from the corresponding authors upon request.

Author contributions

J. Z. wrote the manuscript. W. W. and J. Z. conducted all the experiments and analyzed all the data. H. Q. and H. Y. helped finalized the draft, while Y. Y. performed all the photoluminescence experiment. X. H., N. W., T. W. and H. H. gave advice on the research and supervised the project.

Conflicts of interest

There are no conflicts to declare.

Acknowledgements

The authors acknowledge the Innovative Research Group Project of the National Natural Science Foundation of China (22208237).

Notes and references

1 P. Naumov, D. P. Karothu, E. Ahmed, L. Catalano, P. Commins, J. Mahmoud Halabi, M. B. Al-Handawi and L. Li, *J. Am. Chem. Soc.*, 2020, **142**, 13256–13272.
2 E. Ahmed, D. P. Karothu and P. Naumov, *Angew. Chem., Int. Ed.*, 2018, **57**, 8837–8846.
3 W. M. Awad, D. W. Davies, D. Kitagawa, J. M. Halabi, M. B. Al-Handawi, I. Tahir, F. Tong, G. Campillo-Alvarado, A. G. Shtukenberg, T. Alkhidir, Y. Hagiwara, M. Almehairbi, L. Lan, S. Hasebe, D. P. Karothu, S. Mohamed, H. Koshima, S. Kobatake, Y. Diao, R. Chandrasekar, H. Zhang, C. C. Sun, C. Bardeen, R. O. Al-Kaysi, B. Kahr and P. Naumov, *Chem. Soc. Rev.*, 2023, **52**, 3098–3169.
4 D. P. Karothu, J. M. Halabi, L. Li, A. Colin-Molina, B. Rodríguez-Molina and P. Naumov, *Adv. Mater.*, 2020, **32**, 1906216.
5 R. Costil, M. Holzheimer, S. Crespi, N. A. Simeth and B. L. Feringa, *Chem. Rev.*, 2021, **121**, 13213–13237.
6 B. B. Rath and J. J. Vittal, *Acc. Chem. Res.*, 2022, **55**, 1445–1455.
7 S. Bhandary, M. Beliš, R. Shukla, L. Bourda, A. M. Kaczmarek and K. Van Hecke, *J. Am. Chem. Soc.*, 2024, **146**, 8659–8667.
8 S. Kobatake, S. Takami, H. Muto, T. Ishikawa and M. Irie, *Nature*, 2007, **446**, 778–781.
9 H. Koshima, N. Ojima and H. Uchimoto, *J. Am. Chem. Soc.*, 2009, **131**, 6890–6891.
10 S. Hasebe, Y. Hagiwara, T. Ueno, T. Asahi and H. Koshima, *Chem. Sci.*, 2024, **15**, 1088–1097.
11 F. Tong, M. Al-Haidar, L. Zhu, R. O. Al-Kaysi and C. J. Bardeen, *Chem. Commun.*, 2019, **55**, 3709–3712.
12 M. Tamaoki, D. Kitagawa and S. Kobatake, *Cryst. Growth Des.*, 2021, **21**, 3093–3099.
13 R. O. Al-Kaysi, L. Zhu, M. Al-Haidar, M. K. Al-Muhannah, K. El-Boubbou, T. M. Hamdan and C. J. Bardeen, *CrystEngComm*, 2015, **17**, 8835–8842.
14 P. Naumov, S. C. Sahoo, B. A. Zakharov and E. V. Boldyreva, *Angew. Chem., Int. Ed.*, 2013, **52**, 9990–9995.
15 R. Medishetty, A. Husain, Z. Bai, T. Runčevski, R. E. Dinnebier, P. Naumov and J. J. Vittal, *Angew. Chem., Int. Ed.*, 2014, **53**, 5907–5911.
16 K. Yuhara and K. Tanaka, *Angew. Chem., Int. Ed.*, 2024, **63**, e202319712.
17 B. B. Rath and J. J. Vittal, *J. Am. Chem. Soc.*, 2020, **142**, 20117–20123.
18 J.-W. Wu, B.-F. Long, M.-F. Wang, D. J. Young, F.-L. Hu, Y. Mi and J.-P. Lang, *Chem. Commun.*, 2022, **58**, 2674–2677.
19 A. K. Bartholomew, I. B. Stone, M. L. Steigerwald, T. H. Lambert and X. Roy, *J. Am. Chem. Soc.*, 2022, **144**, 16773–16777.
20 J. Lin, J. Zhou, L. Li, I. Tahir, S. Wu, P. Naumov and J. Gong, *Nat. Commun.*, 2024, **15**, 3633.
21 P. P. Ghate, C. J. Perry, V. Carta, I. Bushnak, Y. J. Almuallem, G. J. Beran, C. J. Bardeen and R. O. Al-Kaysi, *Cryst. Growth Des.*, 2024, **24**, 7695–7703.
22 K. Lam, V. Carta, M. Almtiri, I. Bushnak, I. Islam, R. O. Al-Kaysi and C. J. Bardeen, *J. Am. Chem. Soc.*, 2024, **146**, 18836–18840.
23 F. Tong, D. Kitagawa, I. Bushnak, R. O. Al-Kaysi and C. J. Bardeen, *Angew. Chem., Int. Ed.*, 2021, **60**, 2414–2423.
24 J. M. Halabi, E. Ahmed, S. Sofela and P. Naumov, *Proc. Natl. Acad. Sci. U. S. A.*, 2021, **118**, e2020604118.
25 W. Xu, D. M. Sanchez, U. Raucci, H. Zhou, X. Dong, M. Hu, C. J. Bardeen, T. J. Martinez and R. C. Hayward, *Nat. Mater.*, 2023, **22**, 1152–1159.
26 J. M. Halabi, M. B. Al-Handawi, R. Ceballos and P. Naumov, *J. Am. Chem. Soc.*, 2023, **145**, 12173–12180.
27 J. Peng, C. Han, X. Zhang, J. Jia, J. Bai, Q. Zhang, Y. Wang and P. Xue, *Angew. Chem., Int. Ed.*, 2023, **62**, e202311348.
28 S. Bhandary, M. Belis, R. Shukla, L. Bourda, A. M. Kaczmarek and K. Van Hecke, *J. Am. Chem. Soc.*, 2024, **146**, 8659–8667.
29 S. Bhandary, M. Beliš, L. Bourda, A. M. Kaczmarek and K. Van Hecke, *Angew. Chem., Int. Ed.*, 2023, **62**, e202304722.
30 X. Yang, L. Lan, L. Li, J. Yu, X. Liu, Y. Tao, Q.-H. Yang, P. Naumov and H. Zhang, *Nat. Commun.*, 2023, **14**, 3627.
31 T. Dang, Z.-Y. Zhang and T. Li, *J. Am. Chem. Soc.*, 2024, **146**, 19609–19620.
32 P. Naumov, S. Chizhik, M. K. Panda, N. K. Nath and E. Boldyreva, *Chem. Rev.*, 2015, **115**, 12440–12490.
33 S. Chizhik, A. Sidelnikov, B. Zakharov, P. Naumov and E. Boldyreva, *Chem. Sci.*, 2018, **9**, 2319–2335.
34 Ž. Skoko, S. Zamir, P. Naumov and J. Bernstein, *J. Am. Chem. Soc.*, 2010, **132**, 14191–14202.
35 A. Khalil, D. P. Karothu and P. Naumov, *J. Am. Chem. Soc.*, 2019, **141**, 3371–3375.
36 M. Li, A. Pal, A. Aghakhani, A. Pena-Francesch and M. Sitti, *Nat. Rev. Mater.*, 2022, **7**, 235–249.
37 X. Liu, J. Hu, J. Yang, L. Peng, J. Tang, X. Wang, R. Huang, J. Liu, K. Liu, T. Wang, X. Liu, L. Ding and Y. Fang, *Adv. Sci.*, 2024, **11**, 2307165.
38 A. J. Thompson, A. I. C. Orué, A. J. Nair, J. R. Price, J. McMurtrie and J. K. Clegg, *Chem. Soc. Rev.*, 2021, **50**, 11725–11740.
39 M. K. Panda, S. Ghosh, N. Yasuda, T. Moriwaki, G. D. Mukherjee, C. M. Reddy and P. Naumov, *Nat. Chem.*, 2015, **7**, 65–72.
40 A. Worthy, A. Grosjean, M. C. Pfrunder, Y. Xu, C. Yan, G. Edwards, J. K. Clegg and J. C. McMurtrie, *Nat. Chem.*, 2018, **10**, 65–69.
41 S. Saha and G. R. Desiraju, *J. Am. Chem. Soc.*, 2017, **139**, 1975–1983.
42 S. Hayashi and T. Koizumi, *Angew. Chem., Int. Ed.*, 2016, **55**, 2701–2704.
43 Q. Chen, B. Tang, K. Ye and H. Zhang, *Adv. Mater.*, 2024, 2311762.
44 S. Bhunia, S. Chandel, S. K. Karan, S. Dey, A. Tiwari, S. Das, N. Kumar, R. Chowdhury, S. Mondal, I. Ghosh, A. Mondal,

B. B. Khatua, N. Ghosh and C. M. Reddy, *Science*, 2021, **373**, 321–327.
45 W. Wu, K. Chen, H. Yu, J. Zhu, Y. Feng, J. Wang, X. Huang, L. Li, H. Hao, T. Wang, N. Wang and P. Naumov, *Chem. Sci.*, 2024, **15**, 9287–9297.
46 J. Guo, J. Fan, X. Liu, Z. Zhao and B. Z. Tang, *Angew. Chem., Int. Ed.*, 2020, **59**, 8828–8832.
47 X. Zhang, H. Sun, K.-H. Low, T. Yu and V. K.-M. Au, *Mater. Chem. Front.*, 2023, **7**, 3332–3339.
48 Y. Huang, H. K. Bisoyi, S. Huang, M. Wang, X. M. Chen, Z. Liu, H. Yang and Q. Li, *Angew. Chem., Int. Ed.*, 2021, **60**, 11247–11251.
49 Z. Zhao, Y. Cai, Q. Zhang, A. Li, T. Zhu, X. Chen and W. Z. Yuan, *Nat. Commun.*, 2024, **15**, 5054.
50 J. Zhu, W. Wu, H. Qi, H. Yu, W. Liang, T. Wang, X. Huang, N. Wang, L. Zhou and H. Hao, *Adv. Opt. Mater.*, 2024, **12**, 2400582.
51 O. V. Dolomanov, L. J. Bourhis, R. J. Gildea, J. A. Howard and H. Puschmann, *J. Appl. Crystallogr.*, 2009, **42**, 339–341.
52 G. M. Sheldrick, *Acta Crystallogr., Sect. A: Found. Crystallogr.*, 2008, **64**, 112–122.
53 M. Lakshmipathi, A. I. Sk, P. K. Kundu, S. Tothadi and S. Ghosh, *Cryst. Growth Des.*, 2023, **23**, 4939–4945.
54 J. Peng, J. Yang, Y. Zhao, A. Li and Y. Shu, *Cryst. Growth Des.*, 2024, **24**, 5269–5275.
55 P. M. Toro, D. H. Jara, A. H. Klahn, D. Villaman, M. Fuentealba, A. Vega and N. Pizarro, *Photochem. Photobiol.*, 2021, **97**, 61–70.
56 X. Ma, P. Li, J. Wang, M. Yin and Y. Zhang, *Cryst. Growth Des.*, 2022, **22**, 4133–4138.
57 H. Wang, P. Chen, Z. Wu, J. Zhao, J. Sun and R. Lu, *Angew. Chem., Int. Ed.*, 2017, **56**, 9463–9467.
58 T. Lu and F. Chen, *J. Comput. Chem.*, 2012, **33**, 580–592.
59 S. Das, S. Saha, M. Sahu, A. Mondal and C. M. Reddy, *Angew. Chem., Int. Ed.*, 2022, **134**, e202115359.
60 S. Li, B. Lu, X. Fang and D. Yan, *Angew. Chem., Int. Ed.*, 2020, **59**, 22623–22630.
61 Y. Ye, D. Wang, Y. Zhang, X. Zhou, H. Du, S. Yang, Y. Bao, H. Hao and C. Xie, *Chem.–Eur. J.*, 2024, e202401171.
62 D. J. Van Dijken, P. Kovaříček, S. P. Ihrig and S. Hecht, *J. Am. Chem. Soc.*, 2015, **137**, 14982–14991.
63 Y. Liu, Q. Zeng, B. Zou, Y. Liu, B. Xu and W. Tian, *Angew. Chem., Int. Ed.*, 2018, **57**, 15670–15674.
64 S. Tang, K. Ye and H. Zhang, *Angew. Chem., Int. Ed.*, 2022, **134**, e202210128.
65 D. P. Karothu, R. Ferreira, G. Dushaq, E. Ahmed, L. Catalano, J. M. Halabi, Z. Alhaddad, I. Tahir, L. Li and S. Mohamed, *Nat. Commun.*, 2022, **13**, 2823.
66 D. P. Karothu, J. M. Halabi, L. Li, A. Colin-Molina, B. Rodríguez-Molina and P. Naumov, *Adv. Mater.*, 2020, **32**, 1906216.